Boletim da Sociedade Astronômica Brasileira, **37**, no. 1, 274-277

The Milky Way disk radial abundance gradient from planetary nebulae using Gaia DR3 data

O. Cavichia[1], H. Monteiro[1], A. R. da Cunha-Silva[1], W. J. Maciel[2], & A. F. S. Cardoso[3]

[1] Instituto de Física e Química, Universidade Federal de Itajubá
Av. BPS, 1303, 37500-903, Itajubá-MG, Brazil e-mail: cavichia@unifei.edu.br
[2] Instituto de Astronomia, Geofísica e Ciências Atmosféricas, Universidade de São Paulo
Rua do Matão, 1226, 05508-090, São Paulo-SP, Brazil
[3] Núcleo Cosmo-Ufes & Departamento de Física, Universidade Federal do Espírito Santo
29075-910, Vitória, ES, Brazil

Abstract. Radial abundance gradients in the Galactic disk are among the most important observational constraints for studying the chemical evolution of the Milky Way and other galaxies. Planetary nebulae (PNe) serve as valuable tracers of Galactic chemical evolution, providing precise abundances for several elements not produced by their progenitor stars. However, PNe radial abundance studies are hampered by the large uncertainties in their distances. In this work, we utilized the *Gaia* DR3 database to derive more accurate distances for a sample of 1,200 Galactic PNe by implementing a matching algorithm to associate *Gaia* sources with the central stars of PNe (CSPNe), based on angular proximity and expected *Gaia* photometric colors and refined by comparing extinction values derived from the Balmer decrement with those obtained from Galactic extinction maps. Our method identified 419 PNe with high-probability matches to *Gaia* sources, with 121 sources with positive parallaxes and relative uncertainties below 15% used to recalibrate the Hα surface brightness–radius relation. Final distances for the 419 PNe were determined using a Bayesian approach that combined *Gaia* parallaxes and surface brightness measurements. For an additional 781 PNe without Gaia counterparts, we provide distances derived solely from the Hα surface brightness–radius relation. Using the new distances, we determined radial abundance gradients in the Galactic disk for O/H and the results indicate a flatter gradient than previously reported, with a notable change in slope around 8 kpc, coinciding with the Milky Way corotation radius.

Resumo. Os gradientes radiais de abundância no disco Galáctico constituem algumas das mais relevantes restrições observacionais para o estudo da evolução química da Via Láctea e de outras galáxias. Nebulosas planetárias (PNe) desempenham um papel fundamental como traçadores da evolução química Galáctica, fornecendo abundâncias precisas de diversos elementos que não são sintetizados por suas estrelas progenitoras. Estudos envolvendo gradientes radiais de abundância em PNe são limitados pelas grandes incertezas associadas às suas distâncias. Neste trabalho, utilizamos os dados do *Gaia* DR3 para derivar distâncias mais precisas para uma amostra de 1,200 PNe Galácticas. Implementamos um algoritmo para associar fontes do *Gaia* às estrelas centrais das PNe (CSPNe), considerando a proximidade angular e as cores fotométricas esperadas, com um refinamento posterior por meio da comparação entre valores de extinção derivados do decremento de Balmer e aqueles obtidos em mapas de extinção Galácticos. O método resultou na identificação de 419 PNe com correspondências de alta probabilidade a fontes do *Gaia*. 121 PNe apresentam paralaxes positivas e incertezas relativas inferiores a 15%, sendo utilizadas para recalibrar a relação entre brilho superficial em Hα e o raio. As distâncias finais das 419 PNe foram obtidas por meio de uma abordagem Bayesiana que combina as paralaxes do *Gaia* com as medidas de brilho superficial. Para outras 781 PNe sem contrapartida no *Gaia*, fornecemos distâncias derivadas exclusivamente da relação brilho superficial em Hα – raio. A partir dessas novas distâncias determinamos os gradientes radiais de abundância no disco Galáctico para O/H. Os resultados indicam um gradiente mais plano do que o relatado anteriormente, apresentando uma mudança significativa na inclinação por volta de 8 kpc, coincidindo com o raio de corotação da Via Láctea.

Keywords. Galaxy: abundances – Galaxy: evolution – planetary nebulae: general

1. Introduction

Radial abundance gradients in the Galactic disk are among the most important observational constraints for studying the chemical evolution of the Milky Way and other galaxies Henry & Worthey (1999). These gradients result from a combination of physical processes occurring since the Galaxy formation, including gas infall, star formation history, radial gas flows, and stellar radial migration (Gibson et al. 2013). In the case of the Milky Way, a significant debate exists in the literature regarding the constancy of the gradient for different galactocentric distances. In the outer regions of the Milky Way ($R > 10$ kpc) a flattening of the radial gradient of the disk is noted by data from different tracers such as open clusters (Lépine et al. 2011; Monteiro et al. 2021; Magrini et al. 2023), H II regions (Esteban et al. 2013), Cepheid stars (Genovali et al. 2014; Minniti et al. 2020), and planetary nebulae (PNe, Maciel & Costa 2009; Stanghellini & Haywood 2018). However, there are discrepancies in the literature regarding these results, as evidenced by studies such as Fernández-Martín et al. (2017); Esteban et al. (2017); Arellano-Córdova et al. (2020); Méndez-Delgado et al. (2022) for H II regions, and Stanghellini & Haywood (2010); Pagomenos et al. (2018) and Bucciarelli & Stanghellini (2023) for PNe, where the gradient is suggested to maintain the same slope across the entire optical disk. Part of the disparity between different studies stems from uncertainties in determining chemical abundances and/or distances.

PNe are the evolutionary endpoints of low- and intermediate-mass stars, serve as valuable tracers of Galactic chemical evolution due to their strong optical emission lines and the fact that some elemental abundances remain unaltered during stellar evolution. Estimating reliable distances for Galactic PNe proves particularly challenging, as no single physical parameter directly depends on the distance. Statistical distance methods have therefore been developed to derive PNe distances (see Frew et al. 2016,

hereafter F16, for a comprehensive review). The statistical distance scale from F16, based on an empirical relation between Hα surface brightness ($S_{H\alpha}$) and the intrinsic radius of the PNe, has made an important improvement in the determination of PNe distances. However, statistical distances are subject to considerable uncertainties, often due to factors of two or more, as discussed by F16. Consequently, trigonometric techniques remain the direct and reliable individual method to determine the distances of the PNe when the parallax errors are small (parallax uncertainty over parallax $f \leq 0.15$, Hernández-Juárez et al. 2024). In this regard, the recent *Gaia* mission (Gaia Collaboration et al. 2016, 2018) has revolutionized the determination of the distances for the Galactic PNe (González-Santamaría et al. 2021; Chornay & Walton 2021).

The *Gaia* DR3 (Gaia Collaboration et al. 2016, 2023a) provides unprecedented astrometric parameters, complemented by photometric and spectroscopic data, for hundreds of CSPNe. Even after *Gaia* observations, statistical distances for PNe will be continuously used, since many PNe will not have *Gaia* distance estimates because of the CSPNe are not well identified or in the cases where the parallaxes have a considerable error. In this regard, statistical distance methods for PNe have been recalibrated by using *Gaia* astrometric data, as demonstrated by Stanghellini et al. (2020); Ali et al. (2022) and BS23. In this work our aim is to revisit the issue of PNe abundance gradients relying on reliable distances determined from astrometric parallaxes provided by Gaia data and from statistical distance scale. We present a recalibration of the PN distance scale from F16 using the best parallaxes available from *Gaia* DR3 (Lindegren et al. 2021), enhancing its ability as a robust distance indicator for the many PNe which will not have *Gaia* distance estimates.

2. Methods

González-Santamaría et al. (2021) developed a method to identify CSPNe in *Gaia* EDR3 based on proximity to the geometric center of the nebula and photometric color. Similarly, Chornay & Walton (2020) and Chornay & Walton (2021) employed a likelihood ratio method to cross-match known PNe with *Gaia* EDR3 sources, using empirically derived positional and color distributions to assess candidate likelihoods. We adopted a procedure in this work similar to González-Santamaría et al. (2021) based on angular proximity and expected Gaia photometric colors, which are indicative of CSPNe temperatures. We further refined the matches by comparing extinction values derived from the Balmer decrement with those obtained from Galactic extinction maps. Our method identified 419 PNe with high-probability matches to Gaia sources. Among these, 121 sources with positive parallaxes and relative uncertainties below 15% were used to recalibrate the Hα surface brightness–radius relation and this calibration enabled us to derive reliable statistical distances for the entire sample.

Based on our analysis, we consider that the case for parallax uncertainty over parallax $f \leq 0.15$ with 121 calibrators (Figure 1) provides the best fit by comparing the distances obtained from the calibration and the distances derived from *Gaia* parallaxes. The adopted Hα surface brightness–radius relation in this case is:

$$\log R_{\rm pc} = (-0.26 \pm 0.03) \times \log S_{H\alpha} - (1.52 \pm 0.03). \quad (1)$$

Final distances for a subsample of 419 PNe were determined using a Bayesian approach that combined the distances from the Hα surface brightness–radius relation as priors and Gaia parallaxes. For an additional 781 PNe without Gaia counterparts, we provide distances derived solely from the Hα surface brightness–radius relation.

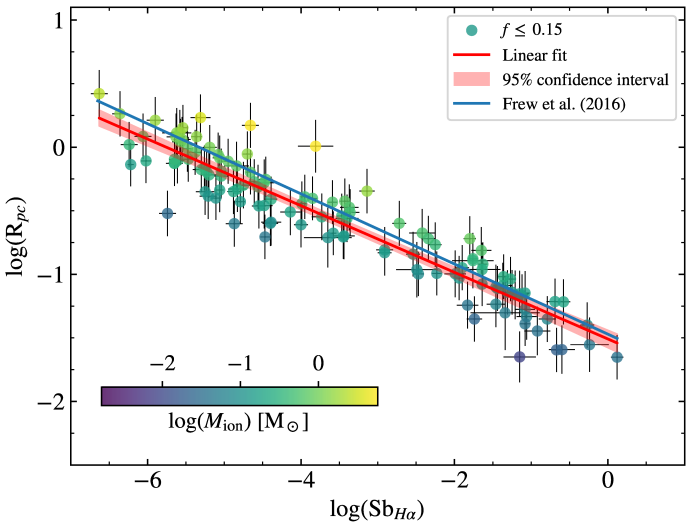

Figure 1. Recalibration of the Hα surface brightness–radius relation based on *Gaia* DR3 parallaxes and considering fractional parallaxes uncertainties $f < 0.15$. The red line and the orange shaded region represent the linear fit and the 95% confidence interval, respectively. The blue line represent the linear fit obtained by F16 for reference. The data are color-coded by the ionized mass.

3. Results

In order to provide a more objective gradient fitting procedure we will employ in this work the same methodology as in Cardoso et al. (2025), where a detailed analysis of the O/H radial abundance gradients derived from the H II region is performed in 154 isolated spiral galaxies observed by the CALIFA survey. The problem of gradient fitting is addressed using a robust unsupervised automatic fitting procedure that employs a bootstrap process on the data to escape local minima. To perform the fit of the abundance radial gradient, we use the Python package `piecewise regression` (Pilgrim 2021). This method simultaneously fits breakpoints positions and linear models for the different fit segments and gives confidence intervals for all the model estimates. The chosen models are a simple linear fit and piecewise linear functions presenting one or two breaks in the radial distributions.

Fig. 2 shows the results of the fitted models and Table 1 summarizes the parameters. In this table the columns refer to the model (linear, one-break and two-break) and the lines the fitted parameters. In the case of the linear model, a_1 and b_1 represent the slope and the intercept. For the one-break and two-break models they represent the parameters of the first segment. a_2 is the slope of the second segment for the one-break and two-break models and a_3 is the slope of the third segment for the two-break model. h_1 and h_2 are the radial positions where a break is detected.

To decide between the models, the Akaike information criterion (AIC, Akaike 1973) is adopted. and we refer to Cardoso et al. (2025) and references therein for more information. The second to last row of Table 1 presents the AIC values for each of the fitted models. The likelihood of a model given the data $\mathcal{L}(m_i|x)$ calculated based on the IAC values (Burnham & Anderson 2002) are presented in the last row of Table 1, where the minimum AIC model is taken as reference.

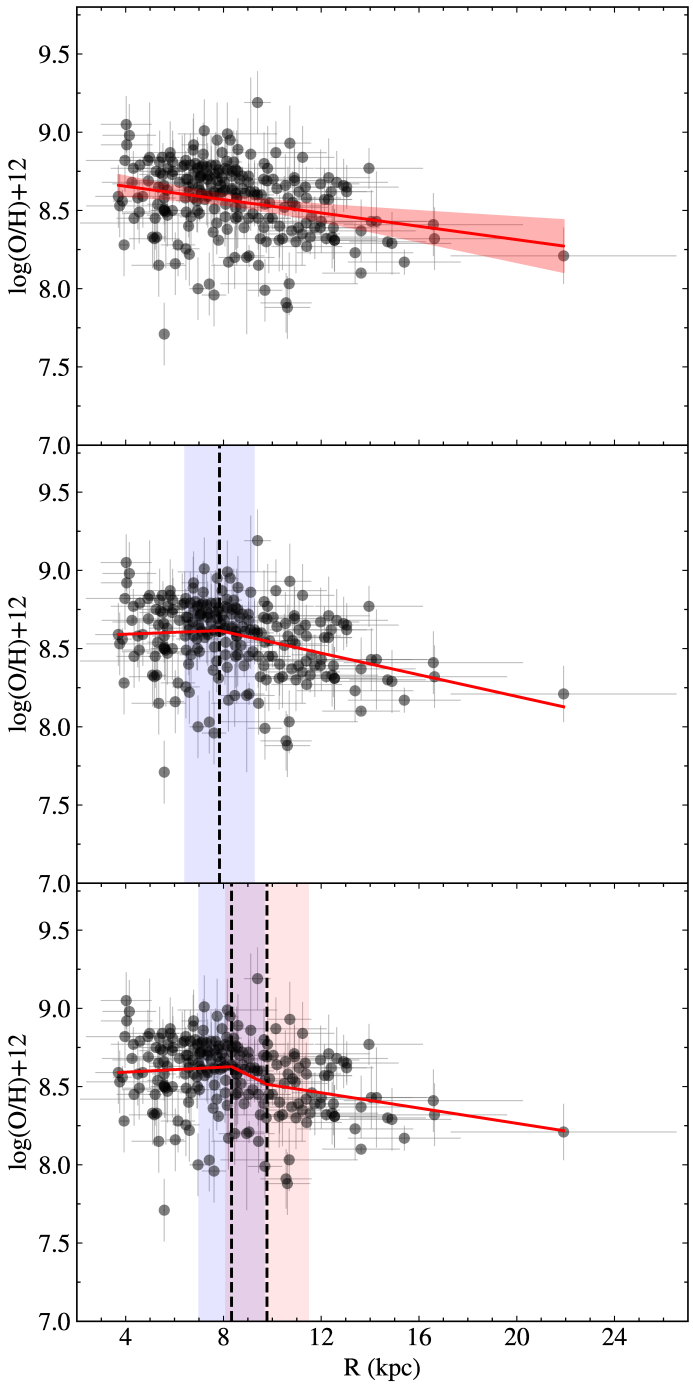

Figure 2. Radial O/H gradient for disk PNe. Top panel: a simple linear fit with the shaded region representing the 95% confidence interval (linear model). Middle panel: a fit considering a break in the radial distribution (one-break model). Bottom panel: a fit with two breaks (two-break model). The vertical dashed lines mark the position of the breaks and the shaded regions the 68% confidence interval.

The most probable model is the one with one break in the radial distribution, presenting the lowest AIC value. In this case, there is a break in the radial distribution at 7.84 ± 1.40 kpc, close to the solar radius. Both models with one and two breaks indicate a flatter gradient inside the solar radius, while outside the solar radius the gradient is steeper. For the one-break model the slopes are 0.009 ± 0.025 and -0.035 ± 0.01 dex/kpc, for the first and second segments, respectively. The two-break model has slopes 0.012 ± 0.017, -0.078 ± 0.112 and -0.024 ± 0.017 dex/kpc, for the first, second and third segments, respectively. In this case, the second segment is the steepest, however with a very short radial range of about 1.5 kpc. Therefore, in this case there is a step in the radial O/H abundance distribution near the Sun position.

However, the alternative models have $\mathcal{L}(m_i|x) > 0.05$, so that the current PNe data do not allow to infer which of the models are the best to fit the data. For this, we need data with smaller uncertainties both in the chemical abundances and distances to confirm the change in slope of the radial O/H gradient near the solar radius.

Table 1. Parameters of the fitted models.

	Model		
Parameters	Linear	One-break	Two-break
a_1 (dex/kpc)	-0.021 ± 0.006	0.009 ± 0.025	0.012 ± 0.017
a_2 (dex/kpc)	–	-0.035 ± 0.010	-0.078 ± 0.112
a_3 (dex/kpc)	–	–	-0.024 ± 0.017
b_1 (dex)	8.74 ± 0.05	8.54 ± 0.15	8.53 ± 0.11
h_1 (kpc)	–	7.84 ± 1.40	8.33 ± 1.30
h_2 (kpc)	–	–	9.78 ± 1.70
AIC	31.32	29.23	30.08
$\mathcal{L}(m_i\|x)$	0.35	1	0.65

To investigate the azimuthal structure in the metallicity distribution, we adopted a procedure similar to Wenger et al. (2019, and references therein), using the software package `pyKrige`[1], which employs kriging (see Feigelson & Babu 2012), to interpolate the distribution of oxygen abundances and to produce an abundance map in the Galactic plane. The interpolation is performed in a grid of Galactic coordinates ranging from -12 to 12 kpc in the x-direction and from -4 to 20 kpc in the y-direction in steps of 1 kpc. The error map is obtained through a 500 Monte Carlo realizations by generating random Gaussian values in the distances and abundances within their uncertainties, adopting the errors as 1-σ confidence interval derived from the PDF. The results are shown in Fig. 3.

4. Conclusions

In Fig. 3 the differences in the interpolated chemical abundances in the O/H map are not very large, but the map revels an azimuthal asymmetry in the distribution. abundances are higher near the solar circle and near the Galactic Center at positive longitudes. The higher abundances near $X = 0$ and $Y = 5$ kpc seem to coincide with end of the expected position of the Galactic bar. This asymmetry in the abundance distribution was also noted by Gaia Collaboration et al. (2023b) using stellar chemical abundances from *Gaia* DR3 data and may be related to radial gas flows induced by the Galactic bar from the OLR to the bar corotation radius, as predicted by chemical evolution models (Cavichia et al. 2014; Kubryk et al. 2015). In the O/H map it is also possible to detect the radial O/H abundance gradient, as beyond the solar circle the abundances drop continuously. The solar circle appears to be a transition region in the pattern of chemical abundance distribution. Inside the solar circle the abundances are higher than in the outside region, creating a bimodal pattern of chemical abundance distribution. This characteristic is consistent with the fits obtained in the one-break and two-break models presented in Fig. 2, where breaks in the radial distribution are detected near the solar circle. For more information we refer to Cavichia et al. (2025).

[1] See `https://github.com/bsmurphy/PyKrige`.

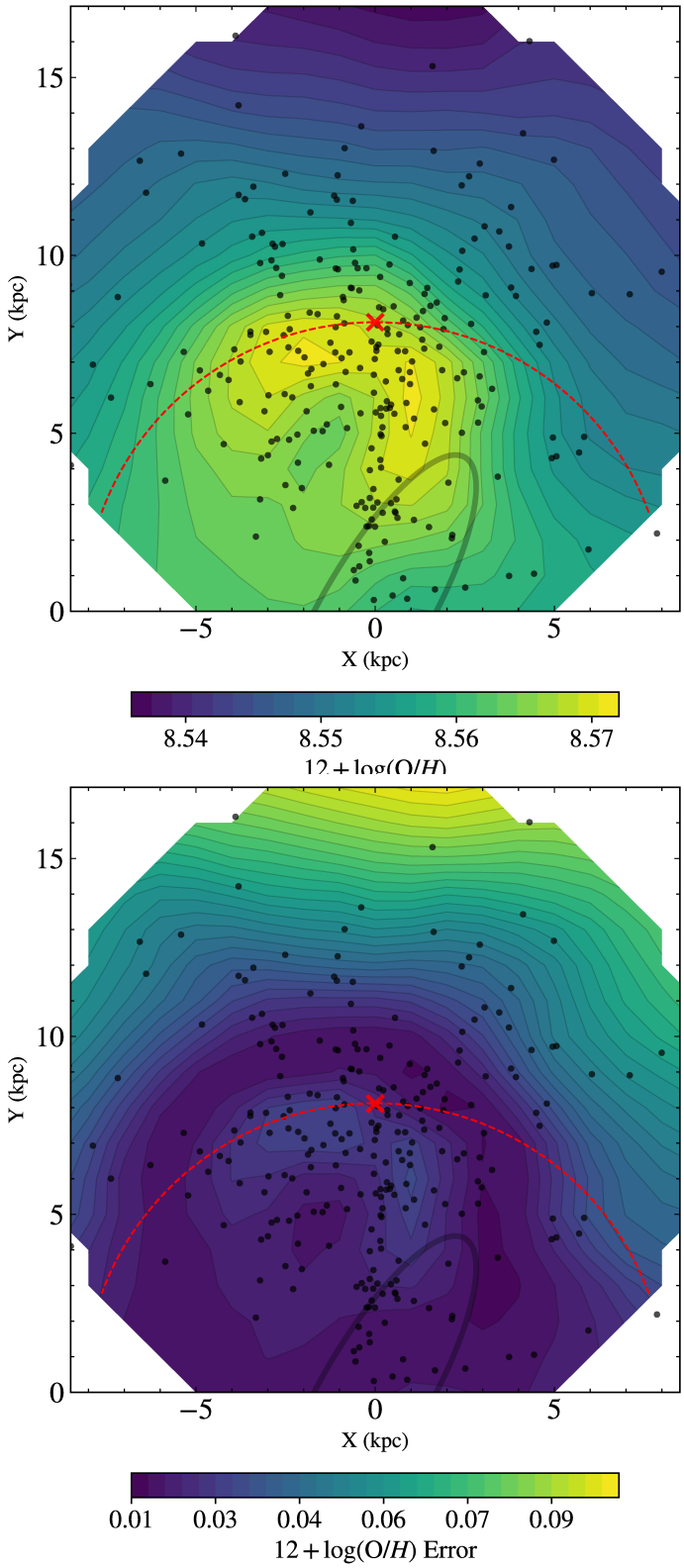

Figure 3. Top: the $\log(O/H) + 12$ abundance map interpolated using the 2D universal kriging algorithm. Bottom: the respective $\log(O/H) + 12$ error map. In both panels the red x marks the position of the Sun and the red dashed semicircunference the solar radius. The gray ellipse centered at the origin represents the position of the Galactic bar after Wegg et al. (2015).

References

Akaike, H., 1973, *Akadémiai Kiadó, Budapest*

Ali, A., Algarni, E., Mindil, A. & Alghamdi, S., 2022, Research In Astronomy And Astrophysics, 22

Arellano-Córdova, K., Esteban, C., García-Rojas, J. & Méndez-Delgado, J., 2020, MNRAS, 496, 1051-1076

Bucciarelli, B. & Stanghellini, L., 2023, A&A, 680, A104

Burnham, K. & Anderson, D., 2002, Model Selection and Multimodel Inference : A Practical Information-Theoretic Approach. (Springer New York : Imprint: Springer)

Cardoso, A., Cavichia, O., Mollá, M. & Sánchez-Menguiano, L., 2025, ApJ, 980, 45

Cavichia, O., Mollá, M., Costa, R. & Maciel, W., 2014, MNRAS, 437, 3688-3701

Cavichia, O., Monteiro, H., Da Cunha-Silva, A., Maciel, W. & Cardoso, A., 2025, arXiv:2509.19239

Chornay, N. & Walton, N., 2020, A&A, 638, A103

Chornay, N. & Walton, N., 2021, A&A, 656, A110

Esteban C., Carigi L., Copetti M. V. F., & et al., 2013, MNRAS, 433, 382

Esteban, C., Fang, X., García-Rojas, J., et al. 2017, MNRAS, 471, 1, 987

Feigelson, E. & Babu, G., 2012, Modern Statistical Methods for Astronomy

Fernández-Martín, A., Péz-Montero, E., Vílchez, J. & Mampaso, A., 2017, A&A, 597, A84

Frew, D., Parker, Q. & Bojičić, I., 2016, MNRAS, 455, 1459-1488

Gaia Collaboration, Prusti, T., de Bruijne, J. H. J., et al. 2016, A&A, 595, A1

Gaia Collaboration, Brown, A., Vallenari, A., Prusti, T. & et al., 2018, A&A, 616, A1

Gaia Collaboration, Vallenari, A., Brown, A., Prusti, T. & et al., 2023a, A&A, 674, A1

Gaia Collaboration, Recio-Blanco A., Kordopatis G., de Laverny P., & et al. 2023b, A&A, 674, A38

Genovali, K., Lemasle, B., Bono, G., Romaniello, & et al., 2014, A&A, 566, A37

Gibson, B., Pilkington, K., Brook, C., Stinson, G. & Bailin, J., A&A, 554, A47

González-Santamaría, I., Manteiga, M., Manchado, A. & et al., 2021, A&A, 656, A51

Henry, R. & Worthey, G., 1999, PASP, 111, 919-945

Hernández-Juárez, D., Rodríguez, M. & Peña, M., 2024, Rev. Mexicana Astron. Astrofis., 60, 227-239

Kubryk, M., Prantzos, N. & Athanassoula, E., 2015, A&A, 580, A127

Lépine, J., Cruz, P., Scarano, S., Barros, D., Dias, W., Pompéia, L., Andrievsky, S., Carraro, G. & Famaey, B., 2011, MNRAS, 417, 698-708

Lindegren, L., Klioner, S., Hernández, J. & et al., 2021, A&A, 649, A2

Maciel, W. & Costa, R., 2009, 254, 38

Magrini, L., Viscasillas Vázquez, C., Spina, L. & et al., 2023, A&A, 669 pp. A119

Méndez-Delgado, J., Amayo, A., Arellano-Córdova, K., Esteban, C., García-Rojas, J., Carigi, L. & Delgado-Inglada, G., 2022, MNRAS, 510, 4436-4455

Minniti, J., Sbordone, L., Rojas-Arriagada, A.,& et al., 2020, A&A, 640, A92

Monteiro, H., Barros, D., Dias, W. & Lépine, J., 2021, Frontiers In Astronomy And Space Sciences, 8, 62

Pagomenos, G., Bernard-Salas, J. & Pottasch, S., 2018, A&A. **615**, A29

Pilgrim, C., Journal Of Open Source Software, 2021, 3859

Stanghellini, L. & Haywood, M., 2010, ApJ, 714, 1096-1107

Stanghellini, L. & Haywood, M., 2018, ApJ, 862, 45

Stanghellini, L., Bucciarelli, B., Lattanzi, M. & Morbidelli, R., 2020, ApJ, 889, 21

Wegg, C., Gerhard, O. & Portail, M., 2015, MNRAS, 450, 4050-4069

Wenger, T., Balser, D., Anderson, L. & Bania,T., 2019, ApJ, 887, 114